

Thermally Driven Topology in Frustrated Systems

Jie-Xiang Yu,^{1,*} Morgan Daly,¹ and Jiadong Zang¹

¹*Department of Physics and Materials Science Program,
University of New Hampshire, Durham, New Hampshire 03824, USA*

Non-trivial topology in a two-dimensional frustrated spin system with the Dzyaloshinskii-Moriya (DM) interaction was investigated by Monto Carlo simulations. At finite temperatures, thermally driven topology was discovered and was found to be dominant at low magnetic field. This topological charge has a quadratic relation with the DM interaction and linear relations with the external magnetic field or the uniaxial magnetic anisotropy. We also proposed a real frustrated system, the Mn-Bi mono-layer film with exceedingly large DM interaction, to enable thermally driven topology. Other topological non-trivial phases in high magnetic field region were also discussed in this real system.

I. INTRODUCTION

Low dimensional magnetic systems have attracted long term interests due to numerous exotic phenomena therein. Its recent marriage to topology has stimulated the development of skyrmion physics. The magnetic skyrmion is a two-dimensional (2D) topological spin texture mainly discovered in B20 chiral magnets.¹⁻⁶ It was first observed in MnSi by small angle neutron scattering and later confirmed in Fe_{0.5}Co_{0.5}Si thin slabs in terms of real space imaging by Lorentz transmission electron microscopy.^{1,2,7} Although in reality, skyrmions are extensively observed and discussed in three dimensional (3D) samples, the concept of skyrmion is still strictly defined in 2D. Skyrmions are uniformly stacked in 3D. Topology of the configuration itself has induced novel properties in skyrmion dynamics and electronic/magnonic transports.

Topology of the skyrmion can be mathematically described in terms of a topological index dubbed the topological charge Q_T ⁸⁻¹⁰, which measures the coverage of a spin configuration onto a unit sphere. Given Θ and Φ the polar and azimuthal angles, respectively, of each spin \mathbf{S} , the topological charge is given by

$$Q_T = \frac{1}{4\pi} \int \sin \Theta d\Theta d\Phi. \quad (1)$$

Geometrically, it simply counts the total solid angle, in units of 4π , enclosed by the configuration. In a compact manifold, Q_T is always an integer number. For a ferromagnetic state, the total solid angle is zero, so that $Q_T = 0$, while for a skyrmion, it completely covers a unit sphere and total solid angle is 4π , so that $Q_T = \pm 1$. In a smooth spin configuration, Q_T can be written in the well adopted form $Q_T = \frac{1}{4\pi} \int d^2r \mathbf{S} \cdot (\partial_x \mathbf{S} \times \partial_y \mathbf{S})$. However, its geometrical definition in Eq. 1 is more universal and applicable even in highly disordered spin configurations.

Skyrmions are well modeled in 2D chiral magnets, in which broken inversion symmetry induces the Dzyaloshinskii-Moriya (DM) interaction. In a finite window of the $B - T$ phase diagram, the skyrmion crystal phase can be figured out. It is not surprising to have nonzero topological charge in this topologically

nontrivial phase. However, as reported by authors' recent work, nonzero topological charge exists in a wide range in the phase diagram.¹¹ Particularly with large magnetic field, the topological charge is nonzero at finite temperatures and peaks around the melting temperature of the ferromagnetic state though it approaches to zero at both low and high temperatures limit. Such emergence of the topological charge is thus driven by thermal fluctuations. In this regime, the spin configuration is completely random, and the topological charge spreads out in the whole lattice. Symmetry consideration suggests that the topological charge is proportional to the external magnetic field B and quadratic order of the DM interaction D^2 . This thermally-driven topology can be detected by thermal magnon Hall effect.¹²⁻¹⁶ Thus, the correspondence between the skyrmion and topological charge is not one to one. The skyrmion definitely leads to nonzero topological charge, but nonzero topological charge does not necessarily indicate the presence of skyrmions. Nonzero topological charge should exist in a variety of 2D spin models with DM interactions.

In 2D chiral magnets, skyrmion phase and thermally driven topological phase coexist when magnetic field is low so that it is hard to distinguish them. In this work, we show the presence of pure thermally driven topological charge in a frustrated antiferromagnetic system. It is a simple hexagonal lattice, which can be regarded as a 2D hexagonal boron nitride structure with buckling, shown in Fig. 1. Two sublattices, labeled by A and B , are in different atomic mono-layers. Magnetic atoms are located at sublattice A and heavy atoms such as $4d$ or $5d$ transition metal with strong spin-orbit coupling (SOC) are located at B . This system has the point group of C_{3v} without inversion symmetry and it is also a prototype of many non-centrosymmetric magnetic monolayer film systems such as Fe/Ir(111) and Fe/Re(0001).¹⁷⁻¹⁹ Then the Hamiltonian in this model is given by

$$\mathcal{H} = \sum_{\langle i,j \rangle} [J\mathbf{S}_i \cdot \mathbf{S}_j + \mathbf{D}_{ij} \cdot (\mathbf{S}_i \times \mathbf{S}_j)] - \sum_i [\frac{1}{2}K_u S_{iz}^2 + BS_{iz}] \quad (2)$$

where in the first term, S_i and S_j are the two nearest neighbor local magnetic moments at sites i and j of sublattice A respectively. Each site has six nearest

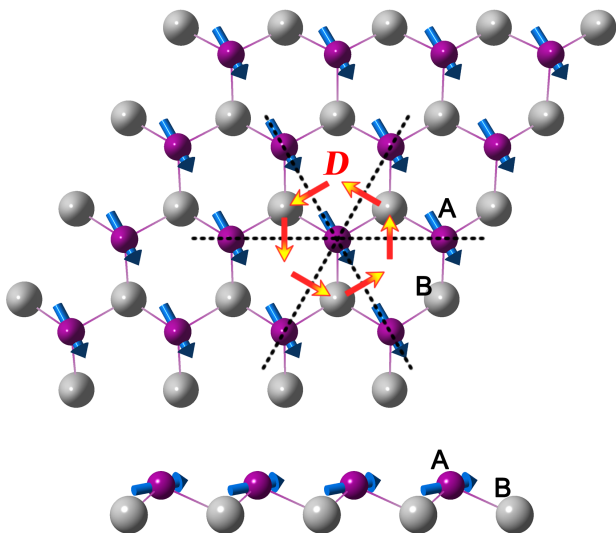


Fig 1: Top view and side view for the crystal structure of a 2D hexagonal lattice with $A-B$ sublattices. A has local magnetic moment. Three dashed lines give six nearest neighbors for one A site. The direction of DM interaction D is given by six arrows.

neighbors. The Heisenberg interaction J originates from the superexchange between two neighboring A sites along $A-B-A$ as well as direct exchange along $A-A$. The direction \hat{D}_{ij} of DM interaction $\mathbf{D}_{ij} = D \cdot \hat{D}_{ij}$ is perpendicular to the bond connecting site i and j according to the Moriya rule²⁰, so it is counterclockwise around one moment, shown in Fig. 1. The second term includes on-site uniaxial magnetic anisotropy K_u and external magnetic field B along z direction.

Antiferromagnetic coupling, namely $J > 0$, in this simple hexagonal lattice leads to a spin frustrated system. It has been reported that the skyrmion phase is, in principle, possible in frustrated magnets.^{21,22} However, such phase exists only at external fields B comparable to the antiferromagnetic exchange J , which is extremely large in most antiferromagnets. Our Monte Carlo simulations reveal that nonzero topological charge takes place at low fields and elevated temperatures. It can be thus easily accessible in experiments. We also proposed a real frustrated system, the Mn-Bi mono-layer film, to enable thermally driven topology. In this material, the DM interaction is exceedingly large so that other topological non-trivial phases at the high field are also discussed.

II. METHOD

A. Monto Carlo Simulations

Numerical Metropolis Monte Carlo simulations were employed²³ iteratively to generate a Markov chain²⁴ of spin configurations, which was then used to derive the

thermal average of the topological charge by employing the Berg formula⁸ with the method mentioned in Ref.¹¹. Periodic boundary conditions were used for 2D hexagonal lattices with sizes 96×96 unless otherwise noted. Local magnetic moment S is normalized so that all the parameters J , D , K_u and B in the Hamiltonian as well as temperature T have the dimensions of energy and J is set as the units of both energy and temperature. Averages over 2.56×10^6 ensembles are performed at each temperature step during the annealing procedure which starts from $10.0J$, a very high temperature.

B. First-principles calculations

The spin-polarized first-principle calculations using the project augmented wave pseudopotential (PAW)^{25,26} implemented in VASP package^{27,28} were performed for calculating electronic and magnetic properties of the Mn-Bi monolayer film. Local density approximation (LDA)²⁹ was employed for the exchange-correlation functional. The wave functions were expanded in plane waves with an energy cutoff of 600 eV throughout calculations. The k points were sampled on a Γ -centered 15×15 mesh in the 2D Brillouin zone of unit cell containing one A-B (Mn-Bi) site. Non-collinear magnetic calculations with SOC are included in total energy calculations for obtaining the magnitude of parameters J , D , K_u in the Hamiltonian.

III. RESULTS AND DISCUSSIONS

A. Topological charge driven by thermal fluctuations

We choose the parameters in the Hamiltonian with $D = 0.40J$, $K_u = 0.20J$ and $B = 0.40J$. The relation between average topological charge Q_T and temperature is shown in Fig. 2. Topological charge density is zero at very low temperature while it has a non-zero region in finite temperature. The valley position is at $T = 0.341J$, with maximum density of $|Q_T|$ about 6.07 per 1000 spins. At very high temperature, Q_T again converges to zero due to the topological triviality of a completely random phase. The same calculations were performed for lattices with sizes ranging from 36×36 to 120×120 . Almost no difference could be found among them, indicating the immunity to the finite-size effect. This robustness of the deep dip of the topological charge should be the scaling-free atomic scale physics.

The valley position of topological charges is close to the phase transition temperature of spin-ordering. Specific heat C_v as a function of temperature is shown in Fig. 2. A discontinuous point appears at $T = 0.315J$, indicating a second-order phase transition. To further understand the relation between topological charge and

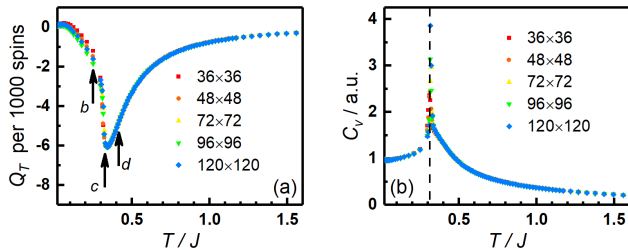


Fig 2: (a) Topological charge density as a function of temperature in the annealing process with various lattice sizes. (b) Temperature dependence of specific heat with various lattice sizes. Three dashed lines labeled *b*, *c* and *d* corresponding to $T = 0.249J$, $0.328J$ and $0.401J$ respectively are for snapshots in Fig. 3

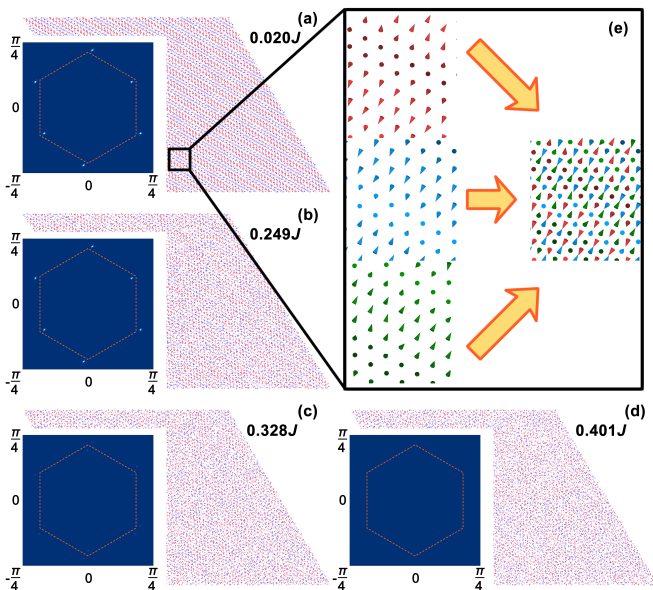


Fig 3: Snapshots and corresponding reciprocal-space images by fast Fourier transform(FFT) at (a) $T = 0.020J$, (b) $T = 0.249J$, (c) $T = 0.328J$, (d) $T = 0.401J$ labeled as dashed line in Fig. 1(a). (e) gives the zoom-in view of (a) to display the combination of three sublattices with helix spin states.

the phase transitions, we took snapshots of spin states at $T = 0.020J$, $0.249J$, $0.328J$ and $0.401J$, respectively.

The same spin-ordering phases take place at very low temperature $T = 0.02J$ [Fig. 3(a)] and low temperature $T = 0.249J$ [Fig. 3(b)], according to both real space spin textures and corresponding fast Fourier transformation (FFT) images. Three neighbor spins in each triangle belongs to three distinct sublattices in the hexagonal lattice, respectively. The second nearest spins are in the same sublattice and tend to be parallel due to nearest neighbor antiferromagnetic coupling. Then each sublattice forms one helical state, shown in Fig. 3(e). The three sublattices have the same q vector so that it is called the single- q state. As a result, in the FFT images, six spots appear in the first Brillouin zone, corresponding

to the $\sqrt{3} \times \sqrt{3}$ spin-reconstruction supercell and the wave vector of each helix corresponds to the offset from each corner of the auxiliary red dashed hexagon in each FFT image. It is obvious that this spin ordering has zero topological charge. It is consistent with previous studies that in antiferromagnets^{30,31} or frustrated systems^{21,22}, no skyrmion or other topological non-trivial spin textures can be found in the low field region.

At $T = 0.328J$ [Fig. 3(c)] which is just above the phase transition temperature $0.315J$, the spin texture is disordered. No spin-ordered texture can be found in real space, corresponding to no spots found in the reciprocal space image. But at that temperature, the topological charge density is -5.91 per 1000 spins, a definitely non-zero value. The same situation happens at higher $T = 0.401J$ [Fig. 3(d)], which is higher than both the phase transition temperature and valley position of topological charges. The topological charge density is -5.09 per 1000 spins while the spin texture is totally disordered. Thus, although the valley position of topological charge is almost the phase transition temperature of spin-ordering, the deep dip of topological charge density at finite temperature does not correspond to any ordered phase because topological charge with the definition in Eq. 1 respects the rotational symmetry, so that it is unable to serve as an order parameter which corresponds to a spin-ordering phase.

It is a system which is topologically trivial at zero temperature but has non-zero topological charge at finite temperature, including temperatures above phase transition temperature. It has the same behavior as the thermal-driven topology in chiral magnets¹¹. According to the definition in Eq. 1, topological charge Q_T respects the spatial inversion symmetry but breaks the time-reversal symmetry. The inversion symmetry bring about a quadratic relation as the lowest order between Q_T and magnetic field D , which is spatial inversion odd; magnetic field B breaks the time-reversal symmetry so that Q_T is proportional to B . Based on this, the magnitude of topological charge relates to magnetic field and DM interactions as:

$$Q_T \propto D^2 B. \quad (3)$$

The same argument applies to current system and a similar relation is held. Fig. 4(a)(c) shows the D dependence of topological charge density. Annealing curves show that the valley positions of topological charge density are almost unchanged while the valley value increases as D increases. According to Fig. 4(c), the value of topological charge density $|Q_T|$ has a quadratic relation with D at $T = 1.49J$. This quadratic relation is also robust all the way to high temperatures. On the other hand, the relation between topological charge density and B is shown in Fig. 4(b)(d). An upward trend in $|Q_T|$ with the increasing B is quite similar with that of $|Q_T| - D$ relation in terms of annealing curves [Fig. 4(b)]. The detailed investigation shows that $|Q_T|$ is proportional to B [Fig. 4(d)].

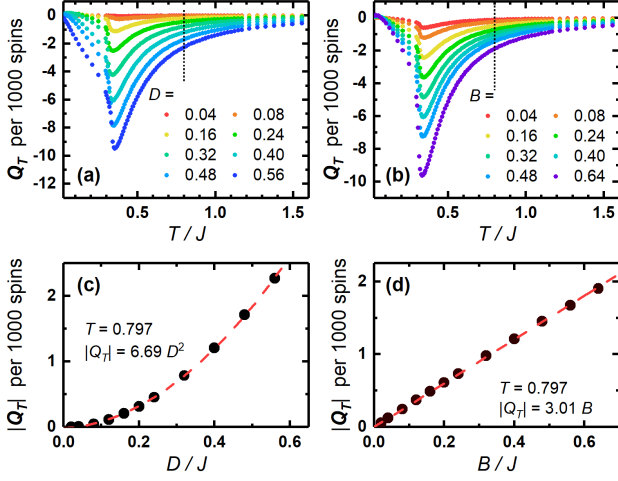


Fig 4: Relationship between topological charge, and DM interaction as well as external magnetic field. Topological charge density as a function of temperature with various (a) D and (b) B . In (a), $B = 0.4J$ and $K_u = 0.2J$ are fixed and in (b), $D = 0.4J$ and $K_u = 0.2J$ are fixed. The value of topological charge density $|Q_T|$ as a function of (c) D and (d) B at $T = 0.797J$ which is shown as the dotted line in (a) and (b).

Although the non-trivial topology in this frustrated system has exactly the same relation with D and B as the thermally driven topology in chiral magnets in high temperature, significant difference, however, appears in low magnetic field and low temperature region. In chiral magnets, skyrmions appear when both temperature and field is low, so non-zero topological charge density can be found in this region. Thermally driven topology is not the only mechanism causing non-trivial topology.¹¹ But for this spin frustrated system, here one can only get the single- q state with trivial topology below phase transition temperature. The only source of non-zero topological charge is the thermal average, so it is a system in which the magnetic topological property is purely contributed by thermally driven topology.

The uniaxial magnetic anisotropy K_u dependence of topological charge was also investigated. The results are shown in Fig. 5(a). Other parameters were fixed at $D = 0.40J$ and $B = 0.40J$. As shown in Fig. 5(a), the valley positions of topological charges increase as K_u is increasing, while the valley values decrease. According to Fig. 5(c) with two magnetic field values $B = 0.10J$ and $0.40J$, the value of topological charge has a linear relationship with K_u in high temperature region. This still obeys the symmetry of $|Q_T|$ since K_u respects both the inversion symmetry and the time-reversal symmetry. According to the linear fitting parameters under two different magnetic field, it can be written as $|Q_T| \propto B(K_u + 1.70)$ or $B(1 + \alpha K_u)$ where $\alpha = 0.59J^{-1}$.

K_u has the similar behavior with external magnetic field at high temperature since the mechanism of K_u can be regarded as an effective magnetic field $B_{eff,i}^{(K_u)} =$

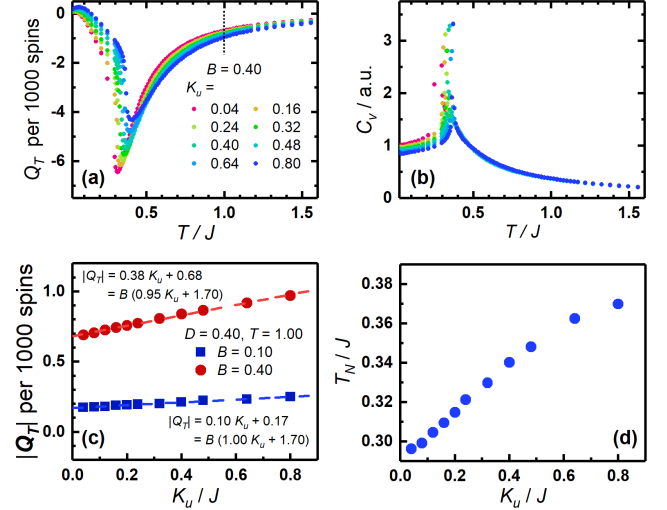


Fig 5: Relationship between topological charge and uniaxial magnetic anisotropy. (a) Topological charge density and (b) specific heat as functions of temperature under various values of K_u with other parameters $D = 0.40J$ and $B = 0.40J$. (c) The value of topological charge density as a function of K_u at $T = 1.00J$ (dotted line in (a)) with two magnetic field values $B = 0.10J$ and $0.40J$, respectively. (d) Phase transition temperature T_N as a function of K_u .

$-\partial \left(\sum_j -\frac{1}{2} K_u S_{jz}^2 \right) / \partial \mathbf{S}_i = K_u S_{iz}$ by the local moment itself applying on that moment. Since this effective field is just an additional magnetic field, the intercept is non-zero when $B \neq 0$. On the other hand, the valley positions of topological charges increase because the phase transition temperature is enlarged by K_u . The K_u dependence of specific heat C_v as a function of temperature is shown in Fig. 5(b). The discontinuous point of C_v move right as K_u increases, indicating the increasing of phase transition temperature. Fig. 5(d) gives the relationship between phase transition temperature T_N and K_u . The intercept value as $0.29J$ is the T_N without magnetic anisotropy and T_N increases about 27% when K_u reaches $0.80J$.

As a result, based on Eq. 3, the thermally-driven topological charge in this system has the relationship

$$Q_T \propto D^2 B (1 + \alpha K_u), \alpha > 0 \quad (4)$$

in high temperature region.

B. Mn-Bi thin film from first principles calculations

This 2D frustrated model is the prototype of many non-centrosymmetric magnetic thin film systems. Here we chose manganese and bismuth as the species of A and B sublattices in this model, respectively. The hexagonal NiAs phase of MnBi is ferromagnetic with its high Curie temperature over 600K and high

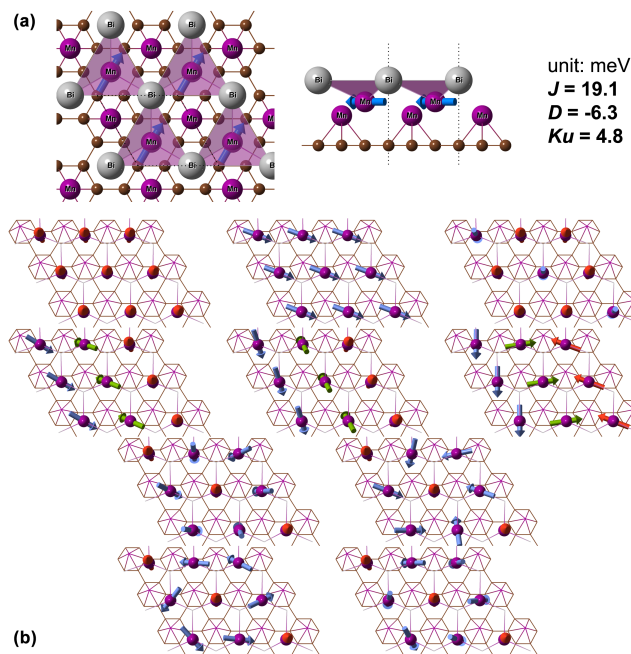


Fig 6: (a) Top view and side view for the structure of 2 ML of Mn (violet balls) and 1 ML of Bi (gray balls) on graphene (brown balls). (b) Ten spin configurations used to build super rank equations for obtaining J , D , K_u . The final result is also displayed.

coercivity with a rectangular hysteresis loop due to large room-temperature perpendicular anisotropy^{32–36}. High Curie temperature is due to strong magnetization, as well as strong exchange interaction, while large perpendicular room-temperature anisotropy originates from strong spin-orbit coupling. Although there is no DM interaction in bulk MnBi because the inversion symmetry is respected, the inversion symmetry can be easily broken in an ultra-thin film. An ideal result is the 2D film with the atomic scale.

To construct Mn-Bi thin films, we chose a graphene sheet as the substrate to stabilize the structure. This is because the in-plane lattice constant of MnBi bulk of 4.28 \AA is quite close to that of $\sqrt{3} \times \sqrt{3}$ graphene lattice of 4.26 \AA . According to the LDA functional calculations, the in-plane lattice constant is fixed at 4.24 \AA in one unit cell (u.c.), which still matches the experimental results. Two mono-layers (MLs) of Mn and one ML of Bi are placed on the graphene sheet. The most stable structure with lowest total energy is shown in Fig. 6(a). Two Mn MLs are located between graphene and Bi ML so that the first ML of Mn is located on the hexagonal hollow of graphene. According to the result of the self-consistent calculations, The first ML of Mn has no magnetization while the local magnetic momentum of the second ML Mn is $3.2\mu_B$.

To get the magnitude of the parameters J , D and K_u , we set ten non-collinear spin configurations on the second ML Mn atoms, shown in Fig. 6(b) and calculate

the total energies for each of them. A set of super rank equations based on the Hamiltonian in Eq. 2 was then built, and eventually all the parameters were obtained. The result is $J = 19.1 \text{ meV/u.c.}$, $D = -6.3 \text{ meV/u.c.}$ and $K_u = 4.8 \text{ meV/u.c.}$, also shown in Fig. 6(a). J is positive, indicating the antiferromagnetic coupling that was expected. Due to the hexagonal lattice, this Mn-Bi thin film system is truly a spin frustrated system. K_u is also positive, so it is uniaxial magnetic anisotropy. D is negative due to the Bi ML located above Mn MLs instead of below them, resulting in the clockwise direction DM interaction around one magnetic moment.

The magnitude of D is quite large. This lattice model value of D can also be converted into the continuum model using $\tilde{D} = D \cdot a / \Omega$ where a is the in-plane lattice constant and Ω is the volume of the unit cell. Therefore, we have $\tilde{D} = -7.0 \text{ mJ/m}^2$, about four times larger than that in the chiral magnet FeGe³⁷. The ratio of D and J is about $1/3$, close to the parameters $D = 0.4J$ in our Monto Carlo numerical simulations mentioned above.

C. Topology in the Mn-Bi thin film

As all necessary parameters in Eq. 2 were obtained in the Mn-Bi thin film, we reformed Monto Carlo simulations to study both the spin ordering and topology in this real system. Fig. 7(a) gives the $B - T$ diagram of topological charge density as a function of the magnetic field B and temperature T . At low magnetic field region, topological charge density is zero at both very low and very high temperature, while there is a ridge near the phase transition temperature. At high temperature region, the absolute value of topological charge densities increases as B increases. Thus, it is consistent with the numerical simulations before, indicating that thermally driven topology dominates the non-trivial topology at low field region in the Mn-Bi thin film.

When $B > 1.1J$, the value of topological charge becomes non-zero at low temperature. According to the snapshot at $B = 1.4J$ shown in Fig. 7(b), two main helical waves, namely double- q , appear in the real space. The two helices form an angle of 120 degrees, resulting in two spots near each corner of the auxiliary hexagon in the reciprocal space. The density of topological charge also shows that although the contribution of topological charge density looks random in the whole lattice, the intersection between two helical waves bring about the considerable negative numbers of topological charges, shown in the dashed circles in Fig. 7(b).

As the magnetic field continues increasing, the number of topological charge grows as well, especially at low temperatures. Around $B = 1.8J$, however, another phase transition takes place. The number of topological charge increase swiftly and has the valley value of over -58 per 1000 atoms at $B = 2.2J$. The snapshot at $B = 2.4J$ gives an honeycomb-like lattice of spin texture, shown in Fig. 7(c). In the reciprocal space, three spots

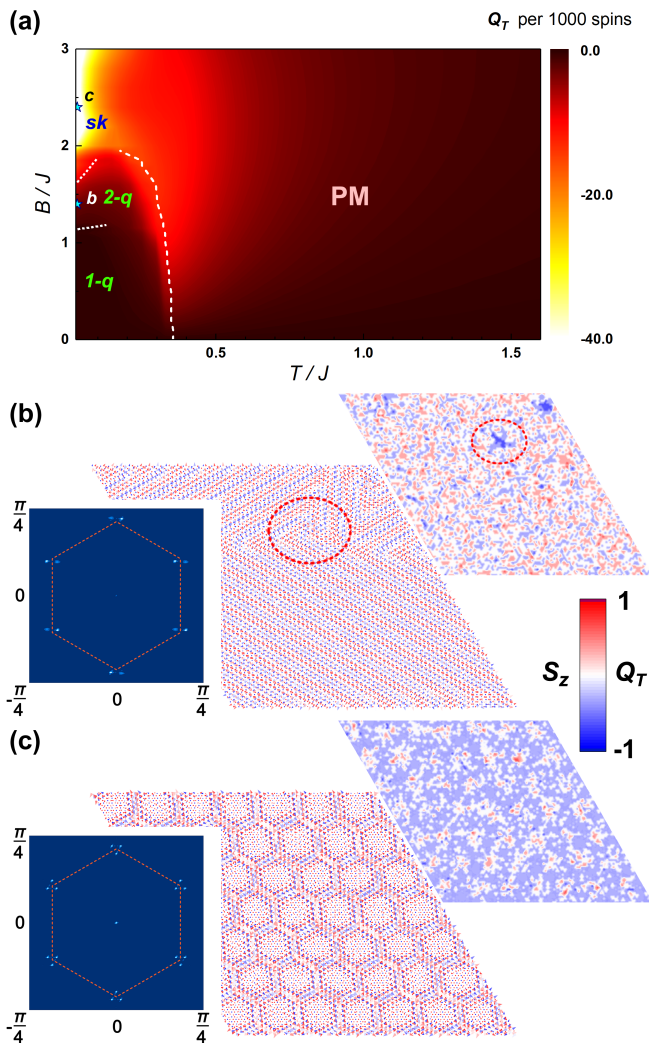


Fig 7: Under Mn-Bi thin film system, (a) the phase diagram of topological charge densities with the magnetic field and temperature dependence. The valley positions are connected by a dashed line. Two white dotted lines divides the region of single- q ($1-q$), double- q ($2-q$) and skyrmion (sk) states, respectively. Star symbols labeled b and c correspond to the snapshots in (b) and (c). Snapshots of spin textures and the corresponding FFT images and distribution of topological charge density with (b) $B = 1.4J$ and (c) $B = 2.4J$ at very low temperature $T = 0.02J$. The color bar gives the colormap of z component of spins and the value of topological charge density.

appear near each corner of the auxiliary hexagon so that there are three helical waves, of which the wave vector has an angle of 120 degrees with other two, in each of the three sublattices. The combination of three helical waves is nothing but the skyrmion crystal lattice, so that each sublattice forms one skyrmion lattice. The total spin texture is the combination of these three skyrmion lattices and the centers of skyrmions together form one hexagonal lattice.

In most skyrmion lattices found in ferromagnets, each skyrmion gives -1 topological charge. Then only 50 skyrmions in the 96×96 lattice, namely about -5 topological charge per 1000 spins, are identified according to the spin texture in Fig. 7(c). It is far from the total value of -55 that the lattice really has. It is because each three neighbor spins forming a triangle are belong to different sublattices. Because of nearest neighbor antiferromagnetic coupling, a large solid angle is formed among them, leading to the large magnitude of the density of topological charge. So that the density of topological charge, shown in 7(c) gives the almost uniformed density with negative value in whole lattice. Thus, the skyrmion phase in this frustrated system has distinct non-trivial topology with skyrmion phase in ferromagnets. Both double- q and skyrmion crystal phase at low temperatures consists with previous studies on frustrated systems^{21,22}.

One should note that the critical magnetic field for skyrmion phase is about $2.0J$. Since $J \sim 20$ meV in the Mn-Bi thin film, the critical field cannot be reached. Furthermore, at least 22 meV of magnetic field, corresponding to $B = 1.1J$, still a giant value, is required to get the double- q state. As a result, under a very wide range of magnetic field strengths, no non-trivial topological phase except for thermally driven topology can be detected in this spin frustrated system, particularly in this Mn-Bi thin film system.

IV. SUMMARY

In conclusion, we have studied the topological properties in a frustrated hexagonal lattice. In a very wide range of low magnetic field, thermally driven topology is the only non-trivial topology under finite temperature. The magnitude of topological charge has the relationship $Q_T \sim D^2 B(1 + \alpha K_u)$ with DM interaction D , magnetic field B and uniaxial magnetic anisotropy K_u in high temperature region. The Mn-Bi thin film system on graphene sheet is such a frustrated system with significant DM interaction. The magnitude of J , D , and K_u in Eq. 2 is identified via first principles calculations. Based on these parameters, a $B - T$ phase diagram of topological charge is obtained. Although both double- q and skyrmion states are found at very high magnetic field region, thermally driven topology is the only non-trivial topological phase under a very wide field range. This makes it easier to be detected by experiments of thermal magnon Hall effect.

This work was supported by the U.S. Department of Energy (DOE), Office of Science, Basic Energy Sciences (BES) under Award No. DE-SC0016424 and used the Extreme Science and Engineering Discovery Environment (XSEDE) under Grant No. TG-PHY170023 for first-principles calculations.

- * Correspond to: jiexiang.yu@unh.edu
- ¹ S. Muhlbauer, B. Binz, F. Jonietz, C. Pfleiderer, A. Rosch, A. Neubauer, R. Georgii, and P. Boni, *Science* **323**, 915 (2009).
 - ² A. Neubauer, C. Pfleiderer, B. Binz, A. Rosch, R. Ritz, P. G. Niklowitz, and P. Böni, *Physical Review Letters* **102**, 186602 (2009).
 - ³ A. Bogdanov and A. Hubert, *Journal of Magnetism and Magnetic Materials* **138**, 255 (1994).
 - ⁴ X. Z. Yu, N. Kanazawa, Y. Onose, K. Kimoto, W. Z. Zhang, S. Ishiwata, Y. Matsui, and Y. Tokura, *Nature Materials* **10**, 106 (2011).
 - ⁵ W. Jiang, X. Zhang, G. Yu, W. Zhang, X. Wang, M. B. Jungfleisch, J. E. Pearson, X. Cheng, O. Heinonen, K. L. Wang, et al., *Nature Physics* **13**, 162 (2016).
 - ⁶ W. Jiang, G. Chen, K. Liu, J. Zang, S. G. te Velthuis, and A. Hoffmann, *Physics Reports* **704**, 1 (2017), <http://www.sciencedirect.com/science/article/pii/S0370157317302934>.
 - ⁷ X. Z. Yu, Y. Onose, N. Kanazawa, J. H. Park, J. H. Han, Y. Matsui, N. Nagaosa, and Y. Tokura, *Nature* **465**, 901 (2010).
 - ⁸ B. Berg and M. Lüscher, *Nuclear Physics B* **190**, 412 (1981).
 - ⁹ N. Nagaosa and Y. Tokura, *Nature Nanotechnology* **8**, 899 (2013), <http://dx.doi.org/10.1038/nnano.2013.243>.
 - ¹⁰ G. Yin, Y. Li, L. Kong, R. K. Lake, C. L. Chien, and J. Zang, *Physical Review B* **93**, 174403 (2016).
 - ¹¹ W.-T. Hou, J.-X. Yu, M. Daly, and J. Zang, *Physical Review B* **96**, 140403 (2017).
 - ¹² S. X. Huang and C. L. Chien, *Physical Review Letters* **108**, 267201 (2012).
 - ¹³ M. Mochizuki, X. Z. Yu, S. Seki, N. Kanazawa, W. Koshibae, J. Zang, M. Mostovoy, Y. Tokura, and N. Nagaosa, *Nature Materials* **13**, 241 (2014).
 - ¹⁴ J. Iwasaki, A. J. Beekman, and N. Nagaosa, *Physical Review B* **89**, 064412 (2014).
 - ¹⁵ M. Hirschberger, R. Chisnell, Y. S. Lee, and N. Ong, *Physical Review Letters* **115**, 106603 (2015).
 - ¹⁶ H. Lee, J. H. Han, and P. A. Lee, *Physical Review B* **91**, 125413 (2015).
 - ¹⁷ S. Heinze, K. von Bergmann, M. Menzel, J. Brede, A. Kubetzka, R. Wiesendanger, G. Bihlmayer, and S. Blügel, *Nature Physics* **7**, 713 (2011).
 - ¹⁸ J. Grenz, A. Köhler, A. Schwarz, and R. Wiesendanger, *Physical Review Letters* **119**, 047205 (2017).
 - ¹⁹ A. Palacio-Morales, A. Kubetzka, K. von Bergmann, and R. Wiesendanger, *Nano Letters* **16**, 6252 (2016).
 - ²⁰ T. Moriya, *Physical Review* **120**, 91 (1960).
 - ²¹ T. Okubo, S. Chung, and H. Kawamura, **108**, 017206 (2012).
 - ²² A. O. Leonov and M. Mostovoy, *Nature Communications* **6**, 8275 (2015), ISSN 2041-1723, <https://www.nature.com/articles/ncomms9275>.
 - ²³ N. Metropolis and S. Ulam, *Journal of the American Statistical Association* **44**, 335 (1949).
 - ²⁴ S. Buhandt and L. Fritz, *Physical Review B* **88**, 195137 (2013).
 - ²⁵ P. E. Blöchl, *Physical Review B* **50**, 17953 (1994).
 - ²⁶ G. Kresse and D. Joubert, *Physical Review B* **59**, 1758 (1999).
 - ²⁷ G. Kresse and J. Furthmüller, *Computation Materials Science* **6**, 15 (1996).
 - ²⁸ G. Kresse and J. Furthmüller, *Physical Review B* **54**, 11169 (1996).
 - ²⁹ J. P. Perdew and A. Zunger, *Physical Review B* **23**, 5048 (1981), <https://link.aps.org/doi/10.1103/PhysRevB.23.5048>.
 - ³⁰ X. Zhang, Y. Zhou, and M. Ezawa, *Scientific Reports* **6**, 24795 (2016).
 - ³¹ B. Göbel, A. Mook, J. Henk, and I. Mertig, *Physical Review B* **96**, 060406 (2017).
 - ³² K. Egashira and T. Yamada, *Journal of Applied Physics* **45**, 3643 (1974), <https://doi.org/10.1063/1.1663831>.
 - ³³ X. Guo, X. Chen, Z. Altounian, and J. O. Ström-Olsen, *Physical Review B* **46**, 14578 (1992).
 - ³⁴ G. Di, S. Iwata, S. Tsunashima, and S. Uchiyama, *Journal of Magnetism and Magnetic Materials* **104-107**, 1023 (1992), ISSN 0304-8853, proceedings of the International Conference on Magnetism, Part II, <http://www.sciencedirect.com/science/article/pii/S030488539290471Y>.
 - ³⁵ P. M. Oppeneer, V. N. Antonov, T. Kraft, H. Eschrig, A. N. Yaresko, and A. Y. Perlov, *Journal of Applied Physics* **80**, 1099 (1996), <https://aip.scitation.org/doi/abs/10.1063/1.362847>.
 - ³⁶ J. B. Yang, K. Kamaraju, W. B. Yelon, W. J. James, Q. Cai, and A. Bollero, *Applied Physics Letters* **79**, 1846 (2001).
 - ³⁷ T. Koretsune, N. Nagaosa, and R. Arita, *Scientific Reports* **5**, 13302 (2015), <https://www.nature.com/articles/srep13302>.